Analysis of influencing factors of excitation parameters for magnetoacoustic tomography with current injection

Su Li(李粟)[1,2], Guoqiang Liu(刘国强)[2,3], Liang Guo(郭亮)[1,†], Wenwei Zhang(张文伟)[2], Chaosen Lu(卢朝森)[4], and Hui Xia(夏慧)[2,3,‡]

[1] *College of Information and Control Engineering, China University of Petroleum, Qingdao* 266580, *China*
[2] *Institute of Electrical Engineering, Chinese Academy of Sciences, Beijing* 100190, *China*
[3] *University of Chinese Academy of Sciences, Beijing* 100049, *China*
[4] *College of Electrical and Automation Engineering, Shandong University of Science and Technology, Qingdao* 266510, *China*

(Received 10 May 2022; revised manuscript received 20 July 2022; accepted manuscript online 5 August 2022)

Magneto-acoustic tomography with current injection (MAT-CI) is a type of hybrid imaging; under the excitation of the static magnetic field, the thermoacoustic effect and the Lorentz force effect will exist at the same time. Therefore, the detected signal is a mixed signal generated by the simultaneous action of the two effects, but the influence of excitation parameters on the two effects is different. In this paper, for objects with different conductivity, the proportion of thermoacoustic signal (TA) and magneto-acoustic signal (MA) in the mixed signal is quantitatively analyzed in terms of three aspects: the magnetic induction intensity, pulse excitation and injection current polarity. Experimental and simulation analyses show that the intensity ratio of MA to TA is not affected when the conductivity varies from 0.1 S/m to 1.5 S/m and other conditions remain unchanged. When the amplitude of the pulse excitation and the strength of the magnetic induction are different, the growth rates of MA and TA are different, which has a significant impact on the proportion of the two signals in the mixed signal. At the same time, due to the Lorentz force effect, MA is affected by the polarity of the injected current and the direction of the static magnetic field. The combination of the static magnetic field and the injected current can not only distinguish the two signals in the mixed signal, but also effectively enhance the intensity of the mixed signal and improve the quality of the reconstructed image.

Keywords: magneto-acoustic tomography with current injection (MAT-CI), thermoacoustic effect, Lorentz force effect, acoustic source

PACS: 43.64.+r, 41.20.Gz, 43.80.+p **DOI:** 10.1088/1674-1056/ac872a

1. Introduction

Studies have found that changes in the electrical properties of biological tissues occur earlier than structural changes, and that there was a significant difference in electrical conductivity between cancerous tissues and normal tissues.[1,2] In medical imaging research aimed at the electrical characteristics of biological tissues, magneto-acoustic tomography with current injection (MAT-CI) is a multi-physical field coupling imaging technology that has the advantage of high-resolution imaging on the basis of ensuring high contrast.[3–8] By detecting changes in electrical conductivity properties, the existence of cancerous tissue can be detected as early as possible, which is of great significance for early screening of cancer.[9–11]

In MAT-CI, two kinds of effects will be generated when pulse excitation is applied to the object in a static magnetic field: one is the Lorentz force effect, which is called the magneto-acoustic effect in this paper in order to distinguish it from the thermoacoustic effect. The charged particles in the conductive object are subjected to the Lorentz force under the action of a static magnetic field and generate magneto-acoustic signals (MA); the other is the thermoacoustic effect, where the object absorbs Joule heat, causing thermal expansion to emit thermoacoustic signals (TA). The actual detected signal is a mixed signal produced by the combined effect of the two effects, which contains rich electrical information inside the object.[8–13] In 2015, Feng *et al.* predicted and observed the simultaneous generation and mixing of TA and MA in water, and further proposed a theory of combining TA and MA for analysis.[14] Zhou *et al.* found that in tissue-like materials, the thermoacoustic effect caused the frequency of the MA to shift to a low level.[15] The existence of the thermoacoustic effect in magneto-acoustic imaging and its influence on magneto-acoustic signals were explored in most of the previous research.[16,17] However, the relationship between the two signals was not quantitatively analyzed in detail. It can be known from the literature[18] that the distribution characteristics of the TA source and MA source are different, and the difference in the proportion of TA and MA in the mixed signal will affect the boundary resolution of the reconstructed image of the mixed signal. In this case, quantitatively distinguishing the signals becomes a method to improve the quality of image reconstruction. In addition, the safety current requirements of biological tissue should be considered when conducting exper-

†Corresponding author. E-mail: guoliang@upc.edu.cn
‡Corresponding author. E-mail: xiahui@mail.iee.ac.cn

© 2023 Chinese Physical Society and IOP Publishing Ltd

iments on biological tissues. Under such conditions, acoustic signals are often weak due to low conductivity of biological tissues, so how to achieve signal enhancement becomes particularly important.

Based on the low conductivity of biological tissue, gel phantom with conductivity in the range of 0.1 S/m–1.5 S/m was selected as the object for simulation and experiment in this paper. Aiming at the thermoacoustic effect and magneto-acoustic effect in MAT-CI, the influence of different excitation parameters on the relationship between the two signals is analyzed step by step. The simulation model was established in COMSOL Multiphysics and used to carry out the coupling numerical calculations of the electromagnetic field forward problem and the sound field forward problem. The values of incentive parameters were refined and the quantitative relationship between TA and MA analyzed. The influence of excitation current polarity and static magnetic field on the detection signal is analyzed, and the aim of signal enhancement and image signal-to-noise ratio improvement is achieved.

2. Principle and method

2.1. Principle

The model schematic diagram of MAT-CI is illustrated in Fig. 1; a conductive object with an isotropic conductivity of $\sigma(\boldsymbol{r})$ is placed in a static magnetic field with flux density $\boldsymbol{B}_0$. A nanosecond-wide pulse excitation current is injected into the object through a pair of electrodes in contact with the object. Since the nanosecond-wide pulse excitation with a duration of less than 1 μs is used in this paper, the thermal diffusion time in biological tissue is much longer than the pulse excitation time, and the thermal conduction can be ignored. The heating function $S(\boldsymbol{r},t)$ is defined as the absorbed energy per unit time and per unit volume

$$S(\boldsymbol{r},t) = \sigma(\boldsymbol{r})|\boldsymbol{E}(\boldsymbol{r},t)|^2, \tag{1}$$

$\boldsymbol{E}(\boldsymbol{r},t)$ is the electric field intensity distribution within the object. The acoustic source of the thermoacoustic effect is the partial derivative of the thermal function $S(\boldsymbol{r},t)$, so the thermoacoustic pressure wave equation[19–21] can be expressed as

$$\begin{aligned}\nabla^2 p(\boldsymbol{r},t) - \frac{1}{c_\mathrm{s}^2}\frac{\partial^2}{\partial t^2}p(\boldsymbol{r},t) &= -\frac{\beta}{C_\mathrm{p}}\frac{\partial S(\boldsymbol{r},t)}{\partial t} \\ &= -\frac{\beta}{C_\mathrm{p}}\frac{\partial \sigma(\boldsymbol{r})|\boldsymbol{E}(\boldsymbol{r},t)|^2}{\partial t},\end{aligned} \tag{2}$$

where $p(\boldsymbol{r},t)$, c_s, β, C_p, and ρ represent the pressure, speed of sound, isobaric volume expansion coefficient, specific heat capacity of tissues, and mass density, respectively.

Under the combined action of alternating electric and magnetic fields, the charged particles in the object are subjected to the Lorentz force, which can be expressed as $F = \boldsymbol{J}(\boldsymbol{r},t) \times \boldsymbol{B}$. The acoustic source of the magneto-acoustic effect[22] is the divergence of the Lorentz force, which is expressed as

$$Q_\mathrm{d} = \nabla \cdot (\boldsymbol{J}(\boldsymbol{r},t) \times \boldsymbol{B}), \tag{3}$$

where $\boldsymbol{J}(\boldsymbol{r},t)$ denotes the current density. Magnetic field $\boldsymbol{B} = \boldsymbol{B}_0 + \boldsymbol{B}(t)$ with external static magnetic field $\boldsymbol{B}_0$, and induced magnetic field $\boldsymbol{B}(t)$ generated by injecting alternating current. According to the electromagnetic characteristics of the tissue,[24] the induced magnetic field generated by the alternating electric field in the object is very small, and the static magnetic field intensity $\boldsymbol{B}_0$ is much larger than the induced magnetic field $\boldsymbol{B}(t)$, that is, $\boldsymbol{B}_0 \gg \boldsymbol{B}(t)$. So the magneto-acoustic pressure wave equation can be expressed as

$$\nabla^2 p(\boldsymbol{r},t) - \frac{1}{c_\mathrm{s}^2}\frac{\partial^2}{\partial t^2}p(\boldsymbol{r},t) = \nabla \cdot (\boldsymbol{J}(\boldsymbol{r},t) \times \boldsymbol{B}_0). \tag{4}$$

The total acoustic source under the excitation of the static magnetic field is the superposition of two types of acoustic sources: one is the divergence of the Lorentz force density, which is called the Lorentz force divergence source, and the second is the time derivative of the Joule heat, which is called the Joule heat source. Combining Eq. (2) with Eq. (4), the total acoustic pressure wave equation can be obtained as

$$\begin{aligned}\nabla^2 p(\boldsymbol{r},t) - \frac{1}{c_\mathrm{s}^2}\frac{\partial^2}{\partial t^2}p(\boldsymbol{r},t) &= \nabla \cdot (\boldsymbol{J}(\boldsymbol{r},t) \times \boldsymbol{B}_0) \\ &\quad - \frac{\beta}{C_\mathrm{p}}\frac{\partial \sigma(\boldsymbol{r})|\boldsymbol{E}(\boldsymbol{r},t)|^2}{\partial t}.\end{aligned} \tag{5}$$

According to Eq. (5), the signals in MAT-CI always contain TA. By analyzing the two source terms, the following qualitative relationships can be initially obtained. (i) The Joule heat source is independent of the static magnetic field. When a static magnetic field is applied, TA remains unchanged, and the intensity of MA is proportional to the intensity of the magnetic field. (ii) The Joule heat source is related to the square of the electric field strength, and the Lorentz force divergence source is linearly related to the first power of the current density. Therefore, when the excitation voltage is increased, the growth rate of TA should be higher than that of MA. (iii) Both the Joule heat source and the Lorentz force divergence source are related to the conductivity. With the increase of the conductivity, the growth rate of the two is the same, and the ratio remains unchanged. (iv) The Joule heat source has no polarity and is independent of the direction of the injected current, whereas the Lorentz force divergence source has a polarity that reverses when the injected current is reversed.

In order to analyze the quantitative relationship between MA and TA under different conditions, the signal intensity ratio P_c can be expressed as the peak-to-peak ratio of the two

signals

$$P_{\mathrm{c}} = \frac{P_{\mathrm{MA}}}{P_{\mathrm{TA}}}, \tag{6}$$

where P_{MA} and P_{TA} are the peak-to-peak values of MA and TA, respectively.

2.2. Simulation model

A cylinder model is established in COMSOL Multiphysics for the object, as shown in Fig. 1, with the radius of the object $r_1 = 0.025$ m. The conductivity of the object is set in the range of 0.1 S/m–1.5 S/m. Referring to the characteristics of biological tissue,[23] the specific heat capacity of the model is $C_{\mathrm{p}} = 3940$ J/(kg·K), and the isobaric volume expansion coefficient is $\beta = 3.84 \times 10^{-4}$ K^{-1}. The whole model is placed in an insulating oil-coupling medium. A time-varying current is injected into the object through a pair of electrode plates A and B. In order to ensure the uniformity of the injected current to each part of the object, the radius of the electrode should be larger than that of the object cross section. The electric current field is used to calculate the electromagnetic field forward problem. Assuming that the flux density of the static magnetic field is only in the z direction, and is uniformly distributed, and the current injection direction is in the x direction, the simulation model can be simplified to a two-dimensional transient axisymmetric model to calculate the sound field problem. PML is used as the boundary condition of the whole model. The sound speed in the object and the coupling medium is set as $c = 1500$ m/s. In the process of sound propagation, conditions such as scattering, reflection and attenuation are not considered.

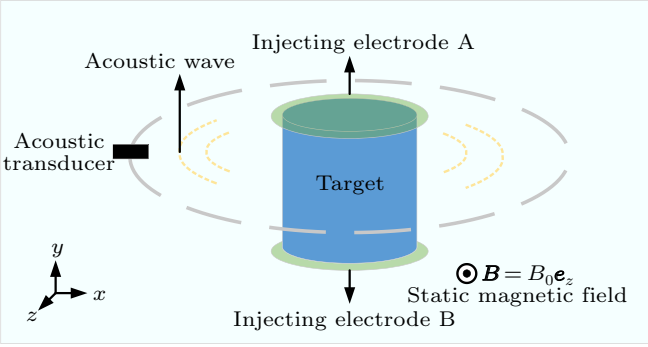


Fig. 1. Simulation model.

2.3. Systems and experiments

The experimental system is divided into three modules as shown in Fig. 2: pulse excitation module, acoustic signal acquisition module and computer control module. The pulse excitation module includes signal generator, pulse excitation source and a pair of silver electrodes. The signal generator controls the working state of the current source by inputting a pulse signal to the pulse current source. During the experiment, a current sensor is used to monitor the excitation current signal in real time. The acoustic signal acquisition module includes a 64-array annular ultrasonic transducer and signal processing system. 64 ultrasonic transducers surround the object to receive acoustic signals, with the signals passed through a 54 dB preamplifier and an adjustable gain secondary amplifier. The gain of the secondary amplifier is regulated by the computer control module, and the acquired acoustic signals are visualized by the signal processing software, which is convenient for analyzing the characteristics of signals.

The size of the cylindrical agar simulant made in the experiment is the same as that of the simulation model with a radius of 0.25 cm. The ultrasonic transducer is placed parallel to the sidewall of the object, and both are immersed in insulating oil. During the experiment, the object can be moved into or out of the static magnetic field by dragging the mobile base. The thermoacoustic effect is studied in the absence of a magnetic field, and the mixed effect is studied in the presence of a magnetic field.

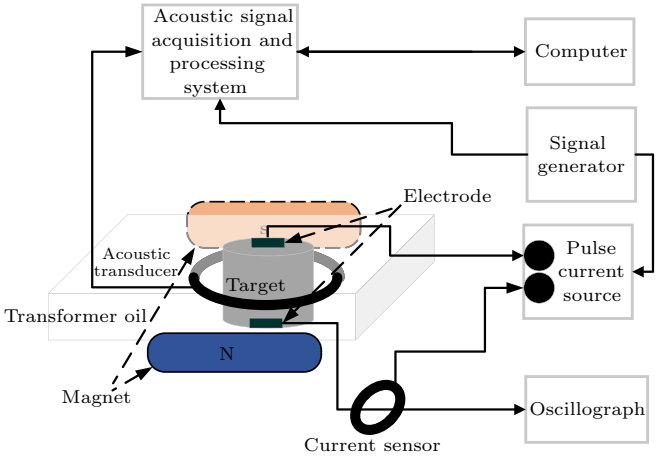


Fig. 2. Experimental system.

3. Numerical analysis

3.1. Influence of tissue conductivity on detection signal

When the excitation pulses are the same, the resistance of the object decreases as the conductivity increases, so the current density flowing through the object increases. Combined with Eqs. (2) and (4), it is found that the intensity of the signal is proportional to the conductivity of the object. The excitation voltage is 1 kV, the pulse width is 500 ns, and when the object is placed in a static magnetic field of 0.4 T and the conductivity changes in the range of 0.1 S/m–1.5 S/m, the peak changes of MA and TA are shown in Fig. 3(a). And figure 3(b) shows the value of P_{c} at different conductivities. After normalizing the acoustic signal, it can be seen that the peaks of MA and TA increase linearly with the increase of the conductivity. Although the growth rate of the two signals is different, P_{c} remains in the range of 0.4–0.45. The experimental results are basically consistent with the simulation results. Therefore, it is concluded

that when the excitation parameters remain constant, conductivity in the range of 0.1 S/m–1.5 S/m does not affect the value of P_c.

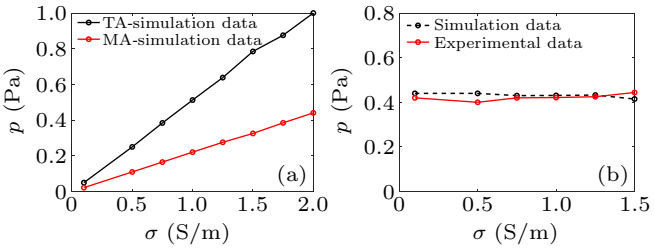


Fig. 3. When the excitation voltage is 1 kV and the intensity of the static magnetic field is 0.4 T: (a) peak variation of the signal under different conductivities, (b) variation of P_c under different conductivities.

3.2. Influence of the magnetic induction intensity on detection signal

Figure 4(a) shows the peak changes of MA and TA under different static magnetic fields when the excitation voltage is 1 kV and the pulse width is 500 ns. The peak of MA increases linearly with the intensity of the static magnetic field. In order to verify the above simulation results, experiments were carried out under magnetic fields with flux densities of 0 T, 0.2 T, 0.4 T, and 1.5 T, respectively. The values of P_c under different static magnetic fields are shown in Fig. 4(b). The experimental results and simulation prediction results both reflect that (i) $\boldsymbol{B}_0 = 0.9$ T, the intensities of the two signals are roughly equal; (ii) $\boldsymbol{B}_0 < 0.9$ T, TA is the main component in the mixed signal, and the intensity of MA is about 0.43–0.5 times that of TA; (iii) $\boldsymbol{B}_0 > 0.9$ T, MA is the main component in the mixed signal, and the intensity of the signal is about 1.6–1.7 times that of TA. From the above analysis, it can be seen that TA is not affected by the intensity of the static magnetic field, which is the key factor affecting MA. Increasing the intensity of the magnetic field is one of the important factors to improve the MA effect.

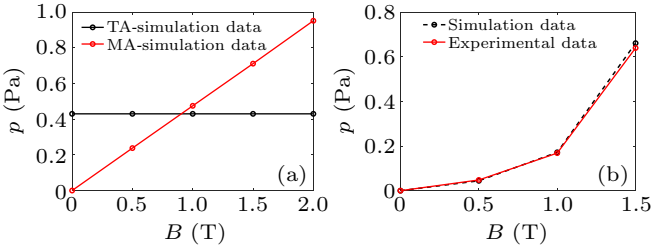


Fig. 4. When the excitation voltage is 1 kV and the conductivity of the object is 0.2 S/m: (a) peak variation of signals under different static magnetic fields, (b) variation of P_c under different static magnetic fields.

3.3. Influence of pulse excitation on the detection signal

For the same object, the amplitude of the injected pulse current can be controlled by changing the excitation voltage. As the excitation voltage increases, the peak value of the injection current increases. When the intensity of the static magnetic field is 0.4 T, the change trend of TA and MA is shown in Fig. 5(a), and the growth rate of TA is higher than that of MA. Figure 5(b) shows the values of P_c under different excitation voltages. The experimental and simulation results show that when the magnetic field intensity is 0.4 T and the excitation voltage is about 0.45 kV–0.5 kV, the intensity of MA is basically equal to that of TA. Comparing the fitting curves, it is found that the intensity of MA has a linear relationship with the excitation voltage, and TA is a square function of the excitation voltage.

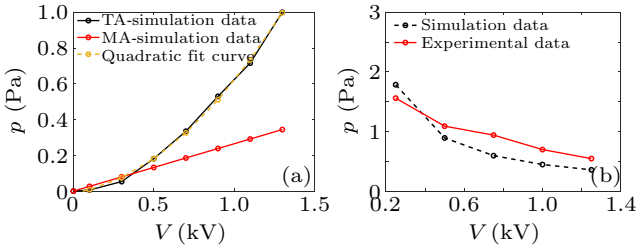


Fig. 5. When the intensity of the static magnetic field is 0.4 T and the conductivity of the object is 0.2 S/m: (a) peak variation of signals under different excitation voltages, (b) variation of P_c under different excitation voltages.

3.4. Influence of injection current polarity on detection signal

The polarity of the injected current is changed by changing the position of the positive and negative plates. Assuming that the upper plate is connected to the positive electrode and the lower plate is connected to the negative electrode, it is forward injection; otherwise, it is reverse injection. Taking the first boundary signal of the object as an example, the red solid line represents the acoustic signal generated by the forward injection, and the black dotted line represents the acoustic signal generated by the reverse injection. As shown in Eq. (5), the charged particles inside the object are affected by the Lorentz force. Due to the orthogonality of $\boldsymbol{B}_0$ and $\boldsymbol{J}(\boldsymbol{r},t)$, when either of the two changes, the phase of MA changes, resulting in time-varying acoustic signals that are not the same in different directions and appear as ∞-type radiation in space. Figures 6(a) and 6(b) are the simulation results of MA and TA under different polarities of injection current, showing that the phase of TA does not change with the polarity of the injection current, but the phase of MA changes 180° with the polarity of the injection current. This again proves that TA is a monopole source, and MA is a dipole source.

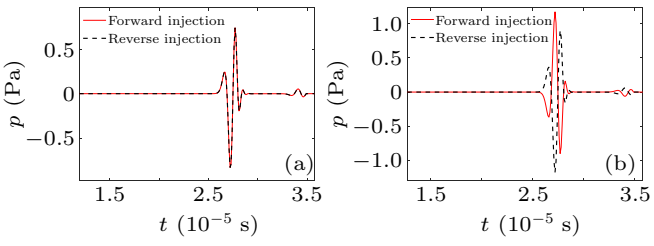


Fig. 6. (a) Simulation comparison of TA under different polarities of injection current, (b) simulation comparison of MA under different polarities of injection current.

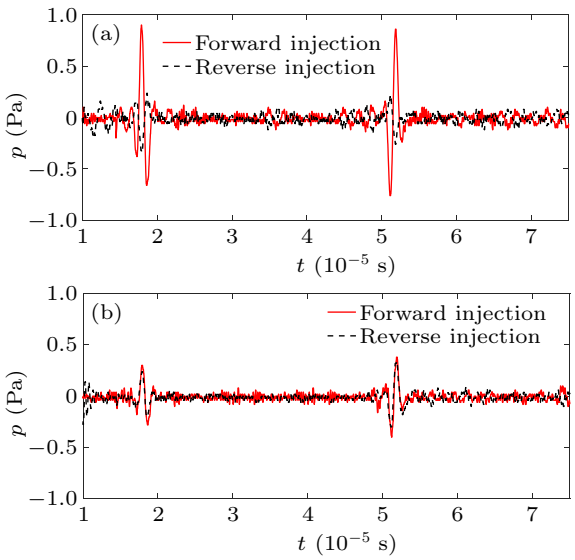


Fig. 7. (a) Experimental comparison of mixed signals under different polarities of injection current, (b) experimental comparison of TA under different polarities of injection current.

Figure 7 is the mixed signal in the experiment. The front boundary is at about 17.78 μs, and the back boundary is at about 51.5 μs. With the sound speed in insulating oil being approximately 1500 m/s, the distance between the two boundaries is calculated to be 5.058 cm, which is the same as the actual size. The signal reflects the boundaries of the conductivity. Figure 7(a) shows mixed signals of the injection current with different polarities under static magnetic field, and figure 7(b) shows TA signals under the same pulse excitation. It is found that the phase of the mixed signals under the different polarities of injection current is opposite, with a difference of 180°. Compared with TA, the phase of the mixed signal during forward injection remains unchanged and the intensity increases, while the phase of the mixed signal during reverse injection is opposite and the intensity decreases. This indicates that MA changes 180° with the change of the polarity of the injection current. In the forward injection, MA has the same phase as TA, which has the effect of signal enhancement; in the reverse injection, the phase of MA is opposite to that of TA, which has the effect of counteracting and weakening.

4. Discussion

During the experiment, using the aforementioned current injection method, 64 ultrasonic probes received signals from multiple angles around the object, as shown in Fig. 8(e). Figure 8(a) is the reconstructed image of thermoacoustic source. The color brightness represents the intensity of the acoustic signal. The radius of the reconstructed image is 0.25 cm, which is the same as the actual size, and can be determined as the acoustic source image. Because the TA have the same phase in each propagation direction, the image contour is complete, but the boundary is less clear due to the influence of SNR. When changing the polarity of the injection current, the positions of the ultrasonic probes and the object were not changed, so the position information contained in the data of each probe did not change, but the amplitude of the mixed signal was changed, being enhanced in the MA and TA co-phase and weakened in the anti-phase. Figures 8(b) and 8(c) are the reconstructed images of the mixed acoustic source after forward and reverse injection of currents under a static magnetic field with 1.5 T, respectively. Signal cancelation occurs when MA and TA are in opposite phase, so that the mixed signal loses much information on the object, which reduces the image reconstruction quality. Figure 8(d) is the MA source image after signal separation. The borders on the left and right sides of the image are clear, and the borders on the upper and lower sides are blurred or even absent. However, due to the error in the placement of probes during the experiment, the object cannot be accurately placed on the same center of the circle, resulting in the upper and lower offset parts being shifted to the right.

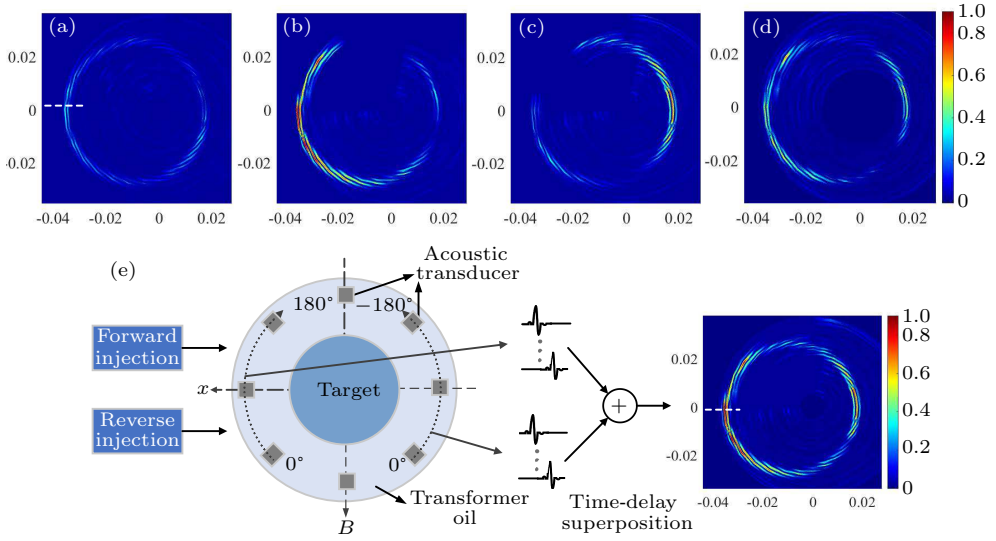


Fig. 8. (a) Source reconstruction image of TA, (b) source reconstruction image of mixed signal with forward injection, (c) source reconstruction image of mixed signal with reverse injection, (d) source reconstruction image of MA after signal separation, (e) image optimization process.

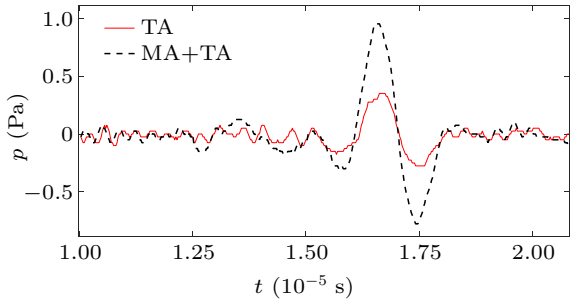


Fig. 9. Amplitude and distribution of acoustic signals at the dotted lines in Figs. 8(a) and 8(e).

As shown in Fig. 8(e), the phase relationship between MA and TA is used to process data under different polarities of injection current. Ensuring that the direction of the static magnetic field remains unchanged, during forward injection, MA and TA are in phase with the positive direction of the magnetic field at an angle of 0° to 180°, and the acoustic signals received by the 32 ultrasonic probes in this direction are extracted; during reverse injection, MA and TA are in phase with the positive direction of the magnetic field at an angle of 0° to −180°, and the acoustic signals received by the 32 ultrasonic probes in this direction are extracted. The extracted acoustic signals are delayed and superimposed, and the two parts of the signal are combined into 64-channel data, which is subjected to low-pass filtering to remove background noise and obtain the fused image. Compared with the reconstructed acoustic image of TA in Fig. 8(a), the reconstructed contour in Fig. 8(e) is clearer and more complete. Figure 9 shows the amplitude of acoustic signals at the dotted lines in Figs. 8(a) and 8(e). It can be seen that the signal intensity after processing is stronger. After calculation, the signal-to-noise ratio is increased by 5.46 dB, which helps to improve the image quality of MAT-CI.

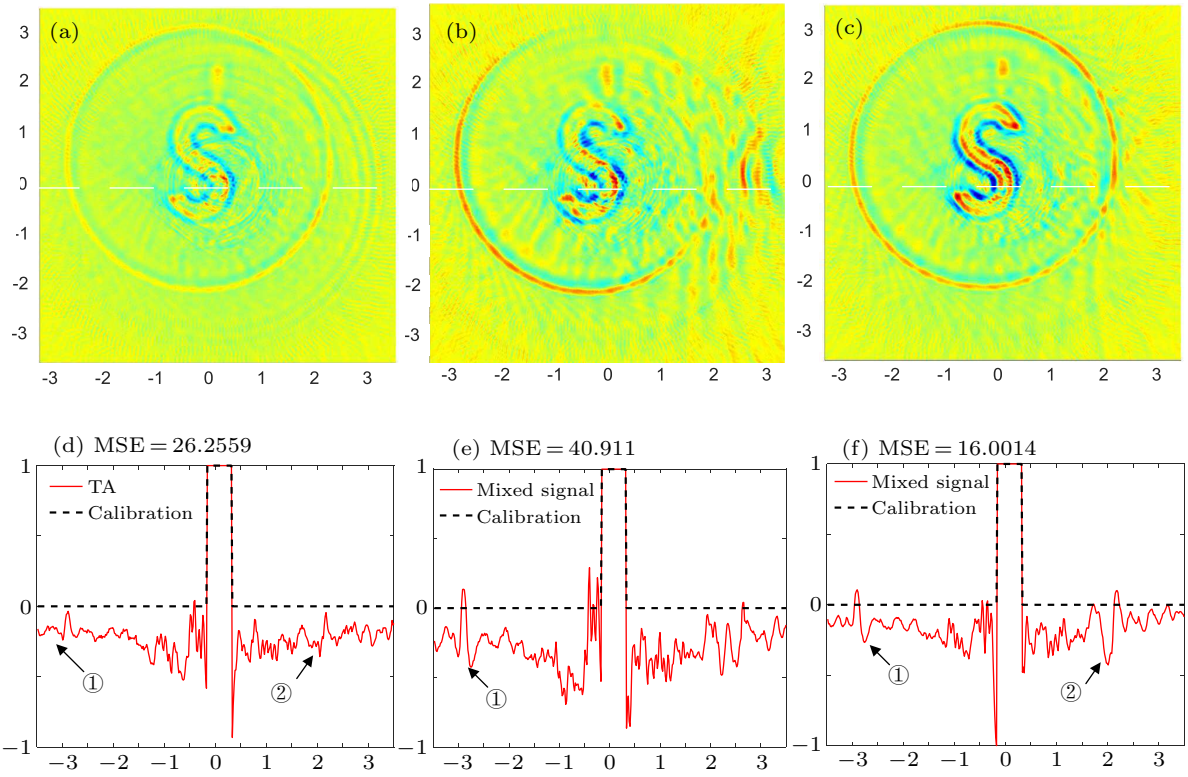


Fig. 10. (a) Source reconstruction image of TA, (b) source reconstruction image of mixed signal with forward injection, (c) optimized source reconstruction image of mixed signal, (d) pixel value at dotted lines in (a), (e) pixel value at dotted lines in (b), (f) pixel value at dotted lines in (c).

The shapes of the anomalous medium in the complex model experiment are set as 'S' and 'TA', and the imaging results are shown in Figs. 10 and 11, where (a), (b), (c) are the source reconstruction image of TA, the source reconstruction image of the mixed signal with forward injection and the optimized source reconstruction image of the mixed signal, respectively. Due to the difference in conductivity between the base phantom and the internal abnormal medium, the three reconstruction results can not only reflect information on the boundary between the base phantom and the abnormal medium, but also show the difference in conductivity between the two through the size of pixel values. Therefore, the quality of the resulting images is determined by the mean square error (MSE) of the pixels in the truncated line. The smaller the MSE, the higher the signal-to-noise ratio (SNR) of the image. Assume that the pixel value of the inner anomalous medium is 1, and the pixel value of the base phantom is 0. The solid red lines in Figs. 10(d)–10(f) and 11(d)–11(f) correspond to the pixel values of the intercepted lines at the same positions in Figs. 10(a)–10(c) and 11(a)–11(c), respectively. The solid black lines represent the ideal normalized pixel curve. Nos. 1 and 2 in Figs. 10(d)–10(f) represent signals at the outer bound-

ary of the base phantom. Due to the directionality of MA in the mixed signal, the signals in the right half of Figs. 10(b) and 11(b) are weakened, resulting in No. 2 in Figs. 10(e) and 11(e) being submerged in noise so that it cannot be distinguished, which loses part of the feature information of the object.

From Figs. 10(a)–10(c) and 11(a)–11(c), it can be found that the reconstructed image in (a) is complete but not clear; the reconstructed image in (b) is incomplete, for example, the valid signals in the right half of the image are submerged in noise and cannot be distinguished, which leads to a lack of feature information of the object; the optimized reconstructed image in (c) not only has a complete and clear boundary, but also has more obvious boundary features of the object. Through the MSE calculation of each imaging result, it is found that the MSE of the optimized reconstructed image is the smallest and the SNR is the highest, which means that the optimization algorithm effectively improves the image quality. Combined with the imaging results of the simple model in Fig. 8, it can be proved that the optimization algorithm proposed in this paper is applicable to both the simple model and the complex model. It not only overcomes the new noise brought by the magnetic field, but also achieves signal enhancement on the basis of the constant excitation current.

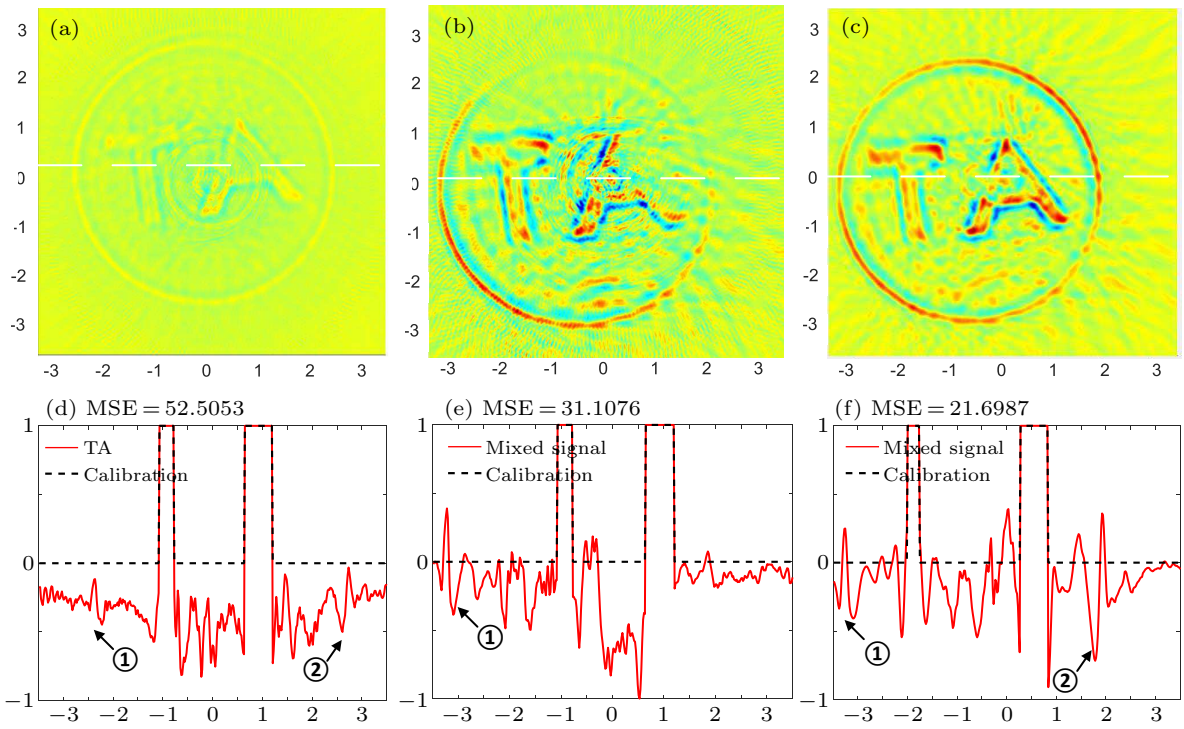


Fig. 11. (a) Source reconstruction image of TA, (b) source reconstruction image of mixed signal with forward injection, (c) optimized source reconstruction image of mixed signal, (d) pixel value at dotted lines in (a), (e) pixel value at dotted lines in (b), (f) pixel value at dotted lines in (c).

5. Conclusion

In this paper, in order to represent normal tissue and cancerous tissue in biological tissue, a low-conductivity material with a conductivity in the range of 0.1 S/m–1.5 S/m is selected as the research object to analyze the influence of excitation parameters. By changing the excitation parameters such as the magnetic induction intensity, pulse excitation and injection current polarity, it is found that the growth rates of MA and TA are different under different excitation voltage and magnetic field intensity. Due to the phase of MA, the signal detection position will directly affect the phase and amplitude of the detection signal. According to the optimal combination method proposed by the signal characteristics of TA and MA, the universality of the algorithm is verified through the verification of complex models. The experimental results show that the boundary of the reconstruction result of TA is fuzzy, and the reconstruction result of mixed signals only contains some image features, while the reconstruction result after using the enhancement algorithm can effectively suppress the noise effect caused by the magnetic field, which not only makes the reconstructed image contain more information about the object, but also makes the boundary of conductivity change clearer. It lays the foundation for the next step of reconstructing high-quality complex model images.

Acknowledgments

This work was funded by the Natural Science Foundation of Beijing (Grant Nos. 7212210 and 3214064), the Natural Science Foundation of China (Grant No. 51937010), and Beijing Science and Technology Commission Project (Grant

No. Z181100003818006).

Project supported by the General Project of Natural Science Foundation of Shandong Province, Research on a New Method of Thermoacoustic Imaging Based on Modular Learning, Project Number: ZR2021ME093.

References

[1] Joines W T, Zhang Y, Li C and Jirtle R L 1994 *Medical Physics* **21** 547
[2] Rahpeima R, Soltani M and Kashkooli F M 2020 *Computer Methods and Programs in Biomedicine* **196** 105606
[3] Li Y H., Liu G Q and Song J X 2020 *J. Appl. Phys.* **128** 174901
[4] Li Y H, Liu G Q, Xia H., Xia Z W and Yang Y J 2018 *IEEE Transactions on Magnetics* **54** 1
[5] Xu L, Yuan X and He B 2007 *IEEE Transactions on Bio-medical Engineering* **54** 323
[6] Liu G Q 2014 *Science Press* (Beijing: Science Press)
[7] Jin X and Wang L V 2006 *Phys Med Biol.* **51** 6437
[8] Ma Q and He B 2008 *IEEE Transactions on Bio-medical Engineering* **55** 813
[9] Zhang S Q, Yin T, Ma R, Ou D P and Liu Z P 2011 *Chinese Journal of Biomedical Engineering* **30** 801
[10] Feng X, Gao F and Zheng Y J 2013 *IEEE MTT-S International Microwave Workshop Series on RF and Wireless Technologies for Biomedical and Healthcare Applications* (IMWS-BIO) 1
[11] Feng X H, Gao F and Zheng Y J 2014 *International Society for Optics and Photonics* 8943
[12] Liu G Q, Xia H, Xia Z W, Li S Q, Yang Y J and Liu Y C N 201410773989.X [2014-12-14]
[13] Hellund E J, Naff J T and Brumfield R C 1963 *Sound: Its Uses & Control* **2** 33
[14] Feng X H, Gao F and Zheng Y J 2013 *Appl. Phys. Lett.* **103** 083704
[15] Zhou X Q, Liu S K, Zhang X S, Yin T and Lin Z P 2018 *Medical and Health Equipment* **39** 5
[16] Li J L, Zhou X Q, Yin T and Liu Z P 2016 *Journal of Biomedical Engineering Research* **35** 145
[17] Yang Y J, Liu G Q and Xia Z W 2017 *Journal of Biomedical Engineering* **34** 21
[18] Yang M, Ma R, Zhang S Q, Zhou X Q, Yin T and Liu Z P 2020 *Chinese Journal of Biomedical Engineering* **39** 295
[19] Jin X and Wang L V 2006 *Phys. Med. Biol.* **51** 6437
[20] Diebold G J, Sun T and Khan M I 1991 *Phys. Rev. Lett.* **67** 3384
[21] Xu M H and Wang L V 2002 *IEEE Transactions on Medical Imaging* **21** 814
[22] Guo L, Liu G Q and Yang Y J 2015 *Appl. Phys. Express* **8** 086601
[23] Tao C J, Song T, Wu S Z and Yan J 2007 *Beijing Biomedical Engineering* **026** 22
[24] Sun Z, Liu G Q, Guo L, Xia H and Wang X L 2016 *Technology & Health Care Official Journal of the European Society for Engineering & Medicine* **24** 683